General Impedance Matching via Doped Epsilon-Near-Zero Media

Ziheng Zhou,[1] Yue Li,[1,†] Ehsan Nahvi,[2] Hao Li,[1] Yijing He,[1] Iñigo Liberal,[3,‡] and Nader Engheta[2,*]

[1] *Department of Electronic Engineering, Tsinghua University, Beijing 100084, China*

[2] *Department of Electrical and Systems Engineering, University of Pennsylvania, Philadelphia, Pennsylvania 19104, USA*

[3] *Department of Electrical and Electronic Engineering, Public University of Navarre, Pamplona 31006, Spain*

(Received 11 November 2019; accepted 22 January 2020; published 3 March 2020)

The emerging technique of photonic doping endows epsilon-near-zero (ENZ) media with a broadly tunable effective magnetic permeability. Here, we theoretically and experimentally demonstrate that a finite-size doped ENZ region counterintuitively behaves as a lumped circuit element, modeled as a controllable series reactance. Based on this concept, a general matching network is constructed to match a load with arbitrary complex impedance, while, interestingly, its operating bandwidth can also be modified by fine-tuning the dopants' properties. To demonstrate the universality of the concept, different kinds of loads are matched, including microwave circuits, antennas, and absorbing particles. Since this general impedance matching technique is not limited to a specific type of load, nor a specific geometry, and can be readily transplanted from microwave to optical regimes, the proposed methodology facilitates impedance matching for maximum usage of power in quite general scenarios, and thus, exhibits promising potential for broad applications.

DOI: 10.1103/PhysRevApplied.13.034005

I. INTRODUCTION

The past decades have witnessed the exciting development of the metamaterial paradigm [1–4], involving synthetic structures that exhibit unconventional properties and advanced functionalities, such as cloaking [5,6], superresolution imaging [7,8], anomalous transmission and reflection [9], analog computing [10], and digital coding [11], to name only a few. Recently, media with a refractive index close to zero i.e., near-zero-index (NZI) media [12,13], have drawn growing interest due to their exotic wave-matter interaction phenomenon. As the permittivity and/or permeability approach zero, the wavelength, as well as the phase velocity of light within the medium, tend to infinity, leading to spatially static, while temporally dynamic, field configurations. These materials with small constitutive relative parameters can give access to a number of intriguing phenomena and applications [13,14], such as supercoupling of waves through arbitrarily shaped channels [15–20], manipulating wave-matter interactions [21,22], and implementing on-chip wave-guiding devices [23]. In addition, NZI media are also introduced into the design of geometry-invariant resonators [24], controlling the emission of quantum emitters [25–27], enhancement of nonlinear effects [28,29], and trapping of light in open resonators [30,31].

The emerging technique of photonic doping [32], where macroscopic dielectric impurities are introduced to an epsilon-near-zero (ENZ) host, provides a new gateway for realizing ENZ media with a designable effective permeability. In fact, to an external observer, an ENZ medium "doped" with one or very few arbitrarily located dielectric particles excites exactly the same external fields (both near and far) as a homogeneous ENZ medium with the designed effective permeability. This includes extreme cases, such as perfect magnetic conductors, with an infinitely large effective permeability, and epsilon-and-mu-near-zero (EMNZ) media, with near-zero effective permeability. Therefore, this intriguing property may lead to some exceptional functionalities unattainable from other material systems.

Here, we utilize doped ENZ building blocks to enable optimal transmission of power, and thus, propose the concept coined "general impedance matching." It is theoretically and experimentally demonstrated that a doped ENZ medium, with an arbitrary cross-section shape, can be modeled exactly equivalent to a series lumped reactive element, despite being a wavelength-size structure containing one or more resonant particles. The specific value of its reactance is directly associated with its effective permeability and can range from negative infinity to positive infinity via tuning of one or more arbitrarily located dopants. Subsequently, general impedance-matching networks are established based on the doped ENZ building blocks. As an important subject in engineering, impedance matching [33]—where a load impedance is transformed to the characteristic impedance of the

*engheta@ee.upenn.edu
†lyee@tsinghua.edu.cn
‡inigo.liberal@unavarra.es

feeding transmission line (or to the complex conjugate of the source impedance)—serves to minimize the reflected power from the load and maximize the transfer of power between the source and the load. Available matching schemes are usually defined for a specific frequency region and customized designs are necessary for different kinds of loads. For example, the networks constructed by lumped inductors [33] and capacitors can offer appreciable degrees of freedom to match electrical devices. However, this method is restricted to low-frequency ranges, since traditional lumped elements need to be much smaller than their operating wavelength. Another popular technique is the quarter-wavelength film [34], which is a standard approach in optics to reduce the reflection of light. However, its applicability is restricted to layered structures with different refractive indices. These structural restrictions do not apply in ENZ media, which can be realized anywhere from the microwave regime to the optical regime via naturally occurring plasmonic materials [35] and artificially synthetic near-zero-index materials [13,15,19,23]. The "infinite" wavelength makes an electrically large area electromagnetically shrink to a "point," where all bodies within it can be described by an effective impedance. Therefore, this technique can be applied to match systems with a complex geometry (which may include bends) that are not necessarily electrically small (when compared with the free-space wavelength).

To demonstrate this concept and its design scheme, exemplary two-component and three-component matching networks based on doped ENZ regions are constructed and analyzed, where we use a microwave component with complex input impedance as the load. As a property of the proposed matching network, a tunable bandwidth is readily obtained by engineering the dispersion of the effective permeability of the doped ENZ material. Three proof-of-concept implementations are presented: (i) the matching of a stepped waveguide, (ii) feeding an aperture antenna, and (iii) efficiently transferring power to an absorbing particle. The first two are experimentally verified by the use of the platform of substrate-integrated photonic doping [36], and the third, associated with the absorbing particle, is numerically demonstrated. The obtained results validate the theory of general impedance matching. Since this technique can be adapted to different frequency regimes and applications, the proposed general impedance-matching scheme sets a new direction in the paradigm of optical circuits, i.e., optical metatronics [37], and it might have important implications in different areas, such as electronics, materials science and energy management.

II. CONCEPT AND THEORY

As conceptually depicted in Fig. 1(a), we consider a two-dimensional (2D) ENZ channel surrounded by perfect electric-conducting (PEC) walls, with arbitrary

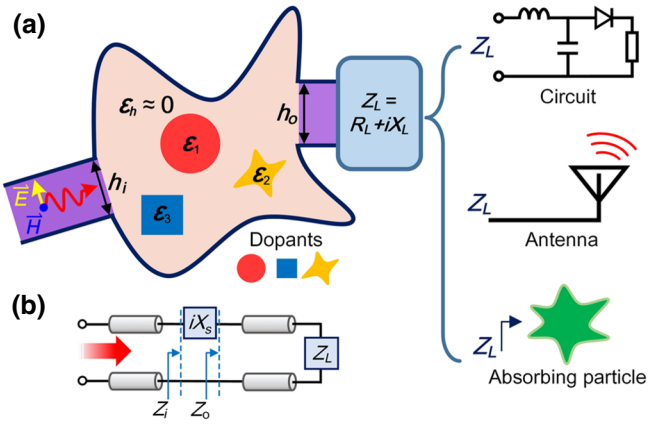

FIG. 1. Conceptual sketch of general impedance matching using doped ENZ regions. (a) A 2D ENZ medium comprising dielectric dopants is introduced within a transmission line to match a load of arbitrary complex impedance Z_L, which can take on various forms in practice, such as circuits and waveguides, antennas, and absorbing particles. Heights of the input and output ports are denoted as h_i and h_o, respectively. Incident wave is polarized with the magnetic field along the out-of-plane axis. (b) Equivalent transmission line model, where the doped ENZ channel is modeled as a series reactance iX_s.

cross-section geometry and area A, containing one or more arbitrarily located dielectric dopants with cross-section area A_d ($d = 1, 2, 3\ldots$). This doped ENZ channel is inserted into a transmission line terminated by a load with an arbitrary complex impedance, Z_L, and excited by an incident wave with the magnetic field polarized along the out-of-plane axis. To obtain the impact of the doped ENZ channel on this configuration, we apply Faraday's law along the boundary of the ENZ channel:

$$\oint_{\partial A} \mathbf{E}\cdot d\mathbf{l} = E_o h_o - E_i h_i = i\omega\mu_0 H \left[\left(A - \sum\nolimits_d A_d\right) + \sum\nolimits_d \iint_{A_d} \psi^d(\mathbf{r})\, ds\right], \tag{1}$$

where E_o and E_i denote the electric field at the output and input ports with heights h_o and h_i, respectively; ω is the operating angular frequency; H is the uniform magnetic field in the ENZ host; and ψ^d is the magnetic-field distribution within a dopant normalized to unity on its boundary. The $e^{-i\omega t}$ time convention is assumed, and we use the fact that the tangential component of the electric field vanishes along the PEC boundary of the channel, and the magnetic field is spatially invariant throughout the ENZ host [15–17]. The impedance seen at the input and output ports of the doped ENZ channel toward the load are denoted as Z_i and Z_o, which are equal to E_i/H and E_o/H, respectively. Therefore, with the help of Eq. (1), the relationship

between Z_i and Z_o yields

$$Z_i = Z_o h_o/h_i - i\omega\mu_0\mu_{\text{eff}}A/h_i, \tag{2}$$

where μ_{eff} is the effective permeability of the doped ENZ channel, which is defined as

$$\mu_{\text{eff}} = \left[A - \sum\nolimits_d A_d + \sum\nolimits_d \iint_{A_d} \psi^d(\mathbf{r})ds\right]/A. \tag{3}$$

As demonstrated in Eq. (2), if the heights of the ports h_i and h_o are set to be equal, the doped ENZ channel contributes a purely imaginary additive impedance, which is proportional to the effective permeability of the doped ENZ region. Equation (2) also implies the interesting physical effect that, although the doped ENZ can be electrically large, it simply behaves as a series lumped impedance component, with the following reactance value:

$$X_s = -\omega\mu_0\mu_{\text{eff}}A/h_i. \tag{4}$$

The equivalent circuit diagram of Fig. 1(a) is displayed in Fig. 1(b). An ENZ region containing no dielectric particles is characterized by $\mu_{\text{eff}} = 1$ and behaves as a series inductance. In contrast, the value of the lumped reactance emulated by the doped ENZ channel can be adjusted to exhibit nontrivial values and dispersion via engineering the effective permeability characteristics by tuning the dopants' properties.

Starting with the doped ENZ material as a cornerstone, we demonstrate the design scheme of general impedance matching. We consider an air-filled parallel-plate waveguide with intrinsic impedance of $\eta_0 = 377\ \Omega$ as the transmission line, while a stepped waveguide with an abrupt change in height from h_1 to h_2 serves as the load with complex input impedance. The port with a height of h_2 is assumed to be terminated by a well-matched wave port. Detailed geometry and impedance characteristics of the stepped waveguide are presented in Section S1 within the Supplemental Material [38], which shows that the input impedance, Z_L, of the stepped waveguide is $(2.1-4.0i)\eta_0$ at $f_p = 5.5$ GHz. To transform impedance Z_L into the intrinsic impedance, η_0, of the transmission line at the design frequency, f_p, we first consider a two-ENZ channel-matching network, which is presented in the left column of Fig. 2(a). To match the load impedance to the transmission line, the required shunt reactance, iX_p, and series reactance, iX_s, in Fig. 2(a) are calculated to be $1.97\eta_0 i$ and $-0.27\eta_0 i$, respectively. The shunt reactance then is replaced by the equivalent series reactance $[iX'_s = \eta_0{}^2/(iX_p) = -0.51\eta_0 i]$ cascaded with quarter-wave transformers (detailed information about the transformation of series impedance to a shunt one is provided in Section S2 within the Supplemental Material [38]), as shown in the middle column of Fig. 2(a). In doing so, the circuit topology may be readily realized by the general impedance-matching scheme, with the series reactance being implemented by a doped ENZ channel, as shown in the right column of Fig. 2(a). Here, the ENZ host for both channels 1 and 2 (Ch.1 and Ch. 2) is assumed to be a plasma with a dispersive permittivity described by the Drude model, $\epsilon_h(f) = 1-(f_p/f)^2$, and, for simplicity, a circular dielectric dopant is adopted. The normalized magnetic field distribution, $\psi^d(r)$, within the circular dopant is given by $J_0(k_d r)/J_0(k_d R_d)$ [32], where $J_n(\cdot)$ denotes the nth order Bessel function of the first kind, $k_d = \sqrt{\epsilon_d}\omega/c$ is the wave number in the dopant (c is the speed of light in vacuum, $\epsilon_d = 88$ is the relative permittivity of the dopant), and R_d represents the radius of the circular dopant. Inserting the expression of the magnetic-field distribution at hand into Eq. (3), we can obtain the effective permeability of the ENZ host comprising circular dopants [39]:

$$\mu_{\text{eff}} = 1 + (1/A) \sum\nolimits_d \{(2\pi R_d/k_d)[J_1(k_d R_d)/J_0(k_d R_d)] - \pi R_d^2\}. \tag{5}$$

Accordingly, the reactance of each doped ENZ channel can be obtained by substituting Eq. (5) into Eq. (4). After obtaining the required reactance from standard circuit analysis, the radii of the dopants can then be found by solving the resulting equation. For the case where each ENZ channel in the two-ENZ-channel network [right column of Fig. 2(a)] contains a single dopant (i.e., dopants with radii R_2 and R_3 are arranged in channels 1 and 2, respectively, while R_1 is assumed zero), the calculated effective permeability of doped ENZ channel 2 for $R_3 = 0.045\lambda_p$ is shown in Fig. 2(b), and the calculated effective permeability of ENZ channel 1 and the simulated transmission coefficient are plotted with green dash-dot lines in Figs. 2(c) and 2(d), respectively. The numerical simulation is carried out by the rf module of the finite-element-method commercial software COMSOL Multiphysics V5.0 [39]. Evidently, total transmission of power is achieved at predesigned frequency f_p, which indicates that the stepped waveguide is perfectly impedance matched.

Next, we demonstrate another powerful property of general impedance matching, the convenient tunability of the bandwidth, which can be realized by engineering the slope of the permeability curve of the doped ENZ channel around the operating frequency. To this end, we fix the parameters of the dopant (R_3) in channel 2, while introducing two dopants, the radii R_1 and R_2 of which can be changed individually in ENZ channel 1. The effective permeability of channel 1 for dopants with different radii are shown in Fig. 2(c) (red dashed line and blue solid line). Specifically, two closely spaced magnetic resonances are clearly observed in the permeability diagram shown in Fig. 2(c); the lower frequency resonance is contributed to

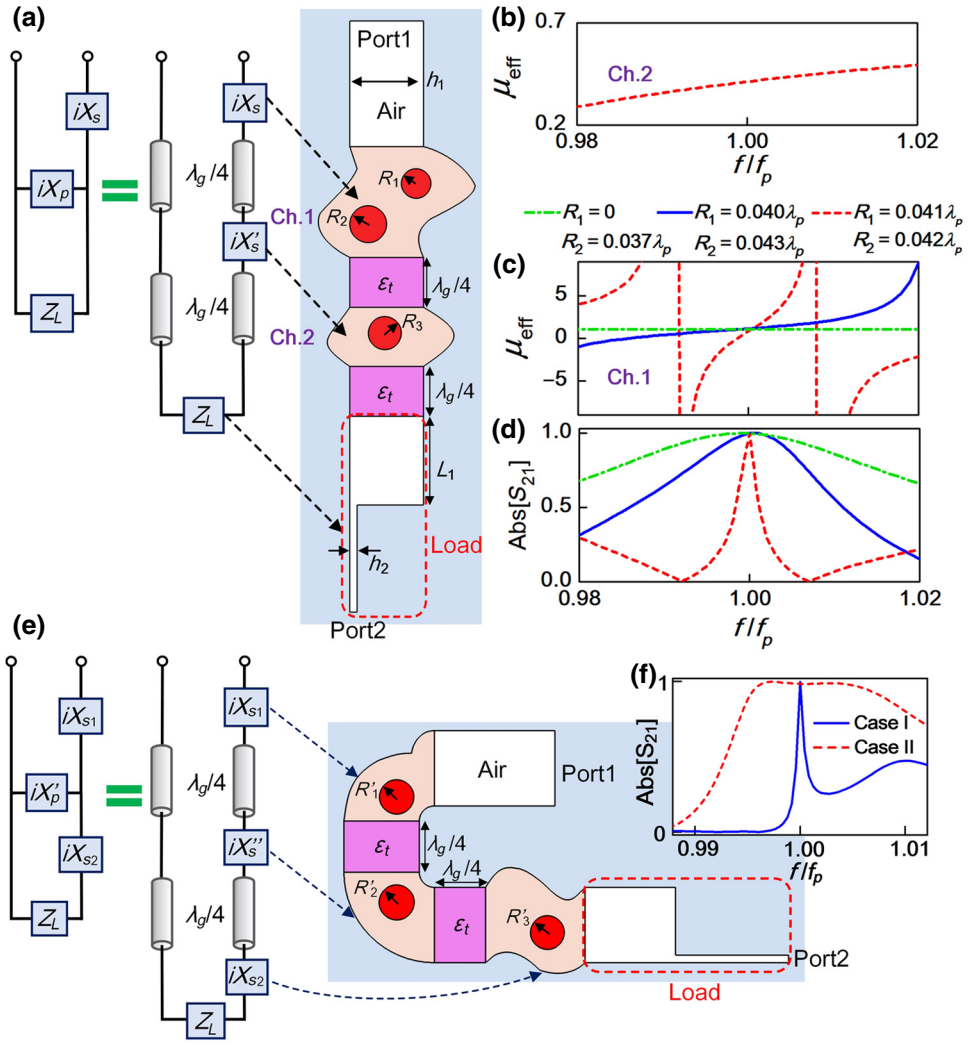

FIG. 2. Bandwidth tailorability with general impedance matching. (a) Equivalent circuit and geometry of a two-ENZ channel-matching network based on photonic doping structures. Cross-section areas of the regions filled with ENZ hosts (denoted by Ch.1 and Ch.2) are $0.073\lambda_p^2$ and $0.039\lambda_p^2$, where λ_p is the free-space wavelength at $f_p = 5.5$ GHz. The relative permittivity of all dopants is chosen as 88, while the quarter-wavelength transmission lines are filled by a material with relative permittivity $\epsilon_t = 1$, e.g., air. The heights of port 1 and port 2 (denoted by h_1 and h_2), and parameter L_1 take values of 10, 1, and 12 mm, respectively. Here, guided wavelength, λ_g, in the transmission line is equal to λ_p. (b) Effective relative permeability of doped ENZ channel 2. (c) Effective relative permeability of channel 1 for different values of the radii of dopants. (d) Simulation results of the transmission coefficients of the two-ENZ channel-matching network. (e) Equivalent circuit and geometry of a three-ENZ channel-matching network based on photonic doping structures. Three ENZ channels comprising dopants (with radii denoted by R_1', R_2', and R_3') are designed with cross-section areas of $0.032\lambda_p^2$, $0.037\lambda_p^2$, and $0.048\lambda_p^2$. (f) Simulation results of transmission amplitudes in Case I, $(R_1', R_2', R_3') = (4.10, 4.28, 4.09)0.01\lambda_p$, and Case II, $(R_1', R_2', R_3') = (4.18, 4.22, 4.11)0.01\lambda_p$.

by the rod with larger radius, while the higher one is provided by the smaller rod. As the difference between the radii of the dopants becomes smaller, the two poles of the permeability function adjacent to f_p get closer, which leads to a stronger dispersion of the lumped reactance, iX_s. In this manner, the matching bandwidth can be engineered into a transmission peak with a higher quality factor [see Fig. 2(d)].

We can also consider a more complicated matching network. A three-ENZ-channel circuit topology with a T-shaped architecture is shown in the left column of Fig. 2(e), where the shunt element is transformed to an equivalent series one, following a procedure similar to that used in the two-element configuration. The architecture of the matching network comprising three doped ENZ channels is shown in the right column of Fig. 2(e). Based on this structure, two cases designed with different radii of the dielectric rods are investigated. In Case I, the reactance values X_{s1}, X_s'', and X_{s2} equal $-1.39\eta_0$, $-0.27\eta_0$, and $5.63\eta_0$, respectively, while, in Case II, X_{s1}, X_s'', and

X_{s2} equal $1.63\eta_0$, $0.22\eta_0$, and $2.17\eta_0$, respectively. It is very interesting to find in Fig. 2(f) that, although the simulated transmission amplitudes of both cases are near 100% at the predesigned frequency, f_p, their bandwidths are dramatically different. The underlying physics is described as follows: to realize the relatively larger (compared with the counterpart in Case II) capacitance value of iX_{s2} for Case I, the doped ENZ channel has to offer a large negative effective permeability [according to Eq. (4)], which features a much steeper slope in the dispersive permeability curve. As a result, through simply tuning the size of the dopants, while leaving other constituents of the network unchanged, we can conveniently control the bandwidth of the impedance matching. We emphasize that, since the electrically large space within index-near-zero media is electromagnetically equivalent to a single point, the behavior of the doped ENZ material and the performance of general impedance matching are independent of the locations of the dopants and the geometry of the ENZ channel.

III. EXPERIMENTAL VERIFICATION

As a proof of concept, we experimentally test the performance of doped ENZ medium to compensate for the reactance of the stepped waveguide, while the intrinsic impedance of the substrate-filled feeding waveguide is designed to be equal to the real part of the load impedance, as shown schematically in the first panel of Fig. 3(a). A rectangular dielectric dopant is chosen for ease of fabrication, and the governing theory of photonic doping for this rectangular dopant has been derived in our earlier work [36]. The input impedance of the load is $(0.92-2.74i)\eta_0$ at $f_p = 5.5$ GHz. Detailed information about calculating the load impedance can be found in Section S1 within the Supplemental Material [38]. To compensate for the input inductance, a series capacitance is needed, corresponding to a doped ENZ channel with a negative effective relative permeability of -0.82. Hence, a dielectric dopant with a relative permittivity of 40 and a cross-section area of 12 $\times$ 2.4 mm^2 ($0.22\lambda_p \times 0.044\lambda_p$, λ_p is the free space wavelength at f_p) is chosen, so as to satisfy this requirement

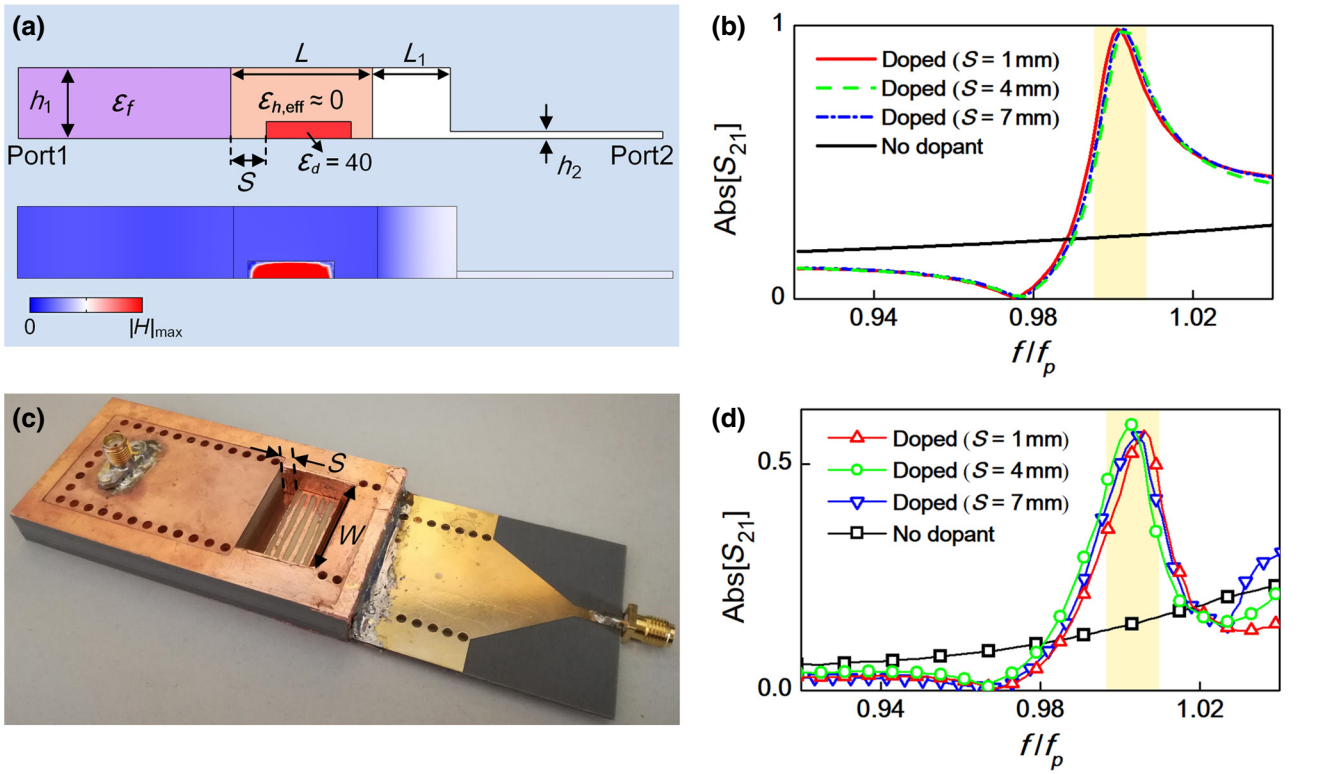

FIG. 3. Experimental verification. (a) The single-ENZ-channel matching network and the distribution of magnetic field magnitude at f_p. The dopant is designed with relative permittivity of 40, loss tangent of 0.001, and a cross-section area of 12 mm $\times$ 2.4 mm ($0.22\lambda_p \times 0.044\lambda_p$). The length L of the doped ENZ channel is 20 mm ($0.37\lambda_p$), the length L_1 of the load is set as 11 mm for the single-ENZ-channel matching, and the relative permittivity of the feeding waveguide ϵ_f is 1.5. The heights h_1 and h_2 of port 1 and port 2 are chosen as 10 and 1 mm, respectively. (b) Simulated transmission coefficients for the dopant placed in different locations and in the absence of the dopant. (c) Photograph of the prototype of the single-ENZ-channel matching network, where a channel with width $W = 27.2$ mm is designed to emulate the plasmonic material following Drude dispersion profile of $\epsilon_{h,\text{eff}}$ with a effective plasma frequency at $f_p = 5.5$ GHz. (d) Measured transmission coefficients for the dopant placed in different positions and in the absence of the dopant.

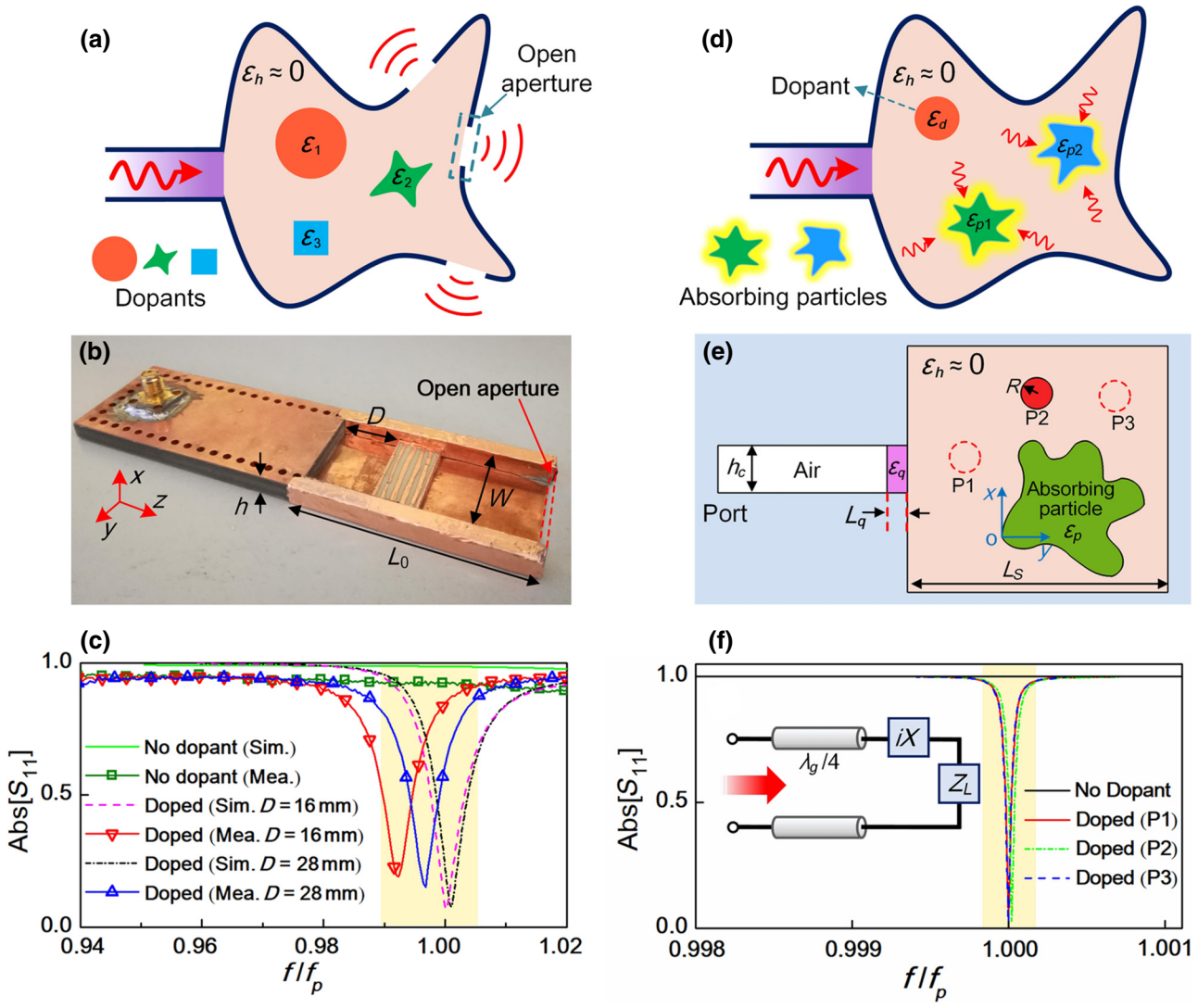

FIG. 4. Applications of general impedance matching. (a) Conceptual sketch of photonic doping to match an antenna. Several apertures are introduced into the walls of the doped cavity, through which an incident-guided wave is transformed into a radiating wave. (b) Photograph of the fabricated aperture antenna matched by a doped ENZ medium. Width W, height h, and length L_0 of the air-filled cavity are set as 27.2, 5, and 55 mm, respectively. Dopant is designed with a size of 27.2 $\times$ 12 $\times$ 2.45 mm^3, relative permittivity of 40, and loss tangent of 0.001. Upper metallic plate of the cavity is not shown here. (c) Measured and simulated reflection coefficients of the antenna with dopant placed at different positions. (d) Conceptual sketch of delivering power to arbitrarily shaped absorbing particles via doped ENZ media. (e) Proposed configuration for matching an absorbing particle with complex permittivity $\epsilon_p = 10 + 0.1i$; detailed geometry information of this absorbing particle is presented in Supplementary Note 4 within the Supplemental Material [38]. The dopant is chosen with permittivity of 40 and radius R of 3.3 mm ($0.061\lambda_p$). Other parameters are $L_s = 53.5$ mm ($0.98\lambda_p$), $h_c = 10$ mm, $L_q = 4.3$ mm, and $\epsilon_q = 11$. (f) Simulated reflection coefficient for the absorbing particle located at different positions. Inset depicts equivalent circuit of the matching scheme.

(analysis of the ENZ channel comprising the rectangular dopant is presented in Section S3 within the Supplemental Material [38]). The simulation result of the distribution of the magnetic-field magnitude at f_p is shown in the bottom panel of Fig. 3(a), which confirms the uniform distribution of the magnetic field within the ENZ host and the complete absence of a standing wave in the input and output waveguides, signifying zero reflection. The simulated transmission amplitude spectrum for the dopant placed in different positions is shown in Fig. 3(b), verifying that the matching performance is independent of the location of the dopant. Our prototype of the single-ENZ channel-matching network, constructed using the planar circuit-board technique, is shown in Fig. 3(c). An air-filled waveguide, operating around its cutoff frequency for its TE_{10} mode, with a width W of 27.2 mm, is employed to emulate a material with a permittivity dispersion described by the Drude model, with a effective plasma frequency

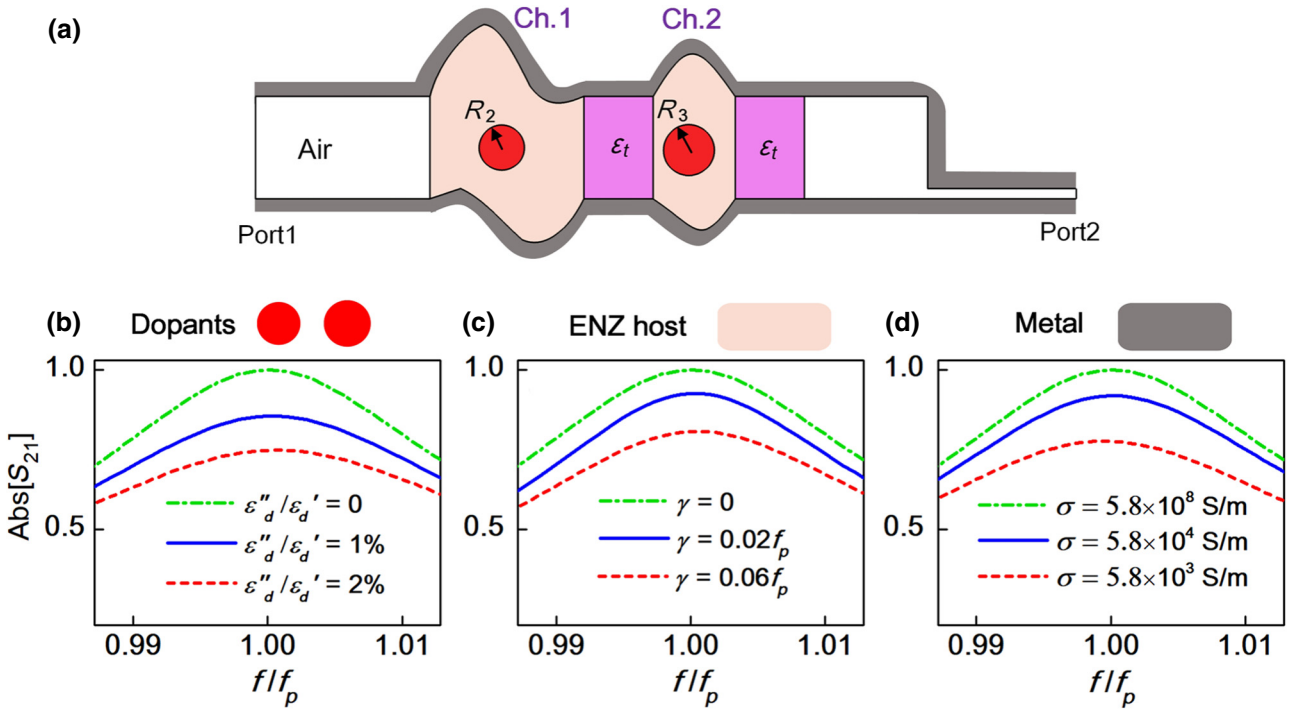

FIG. 5. Numerical investigation of the influence of material loss. (a) Geometry of a two-element matching network, similar to those in Fig. 2(a) (radii of dopants in Ch. 1 and Ch. 2 are $0.037\lambda_p$ and $0.045\lambda_p$, respectively), but considering the influence of loss of dopants, ENZ media, or surrounding metallic walls, which are shown in (b)–(d), respectively.

at its cutoff frequency [40], that is, $\epsilon_{h,\mathrm{eff}} = 1-(f_p/f)^2$ and $f_p = c/(2W)$. The thin metal strip fenced around the dopant is introduced to suppress undesired coupling to TM modes in the ENZ channel [32], while the metallized vias arranged at the two sides of the feeding waveguide, as well as the stepped waveguide, provide the perfect electric conductor boundary. Additional details on the assembly procedure are presented in Appendix A. The measurement results are shown in Fig. 3(d), where the transmission peak is consistently observed around f_p for the dopant located with different displacements S. Lower transmission amplitudes than those in simulations are caused by the dielectric loss of the dopant and substrate. This conclusion is corroborated by the parametric study on the influence of the loss presented in Fig. S4 within the Supplemental Material [38].

IV. APPLICATIONS OF GENERAL IMPEDANCE MATCHING

In previous sections, we shown, theoretically and experimentally, an example of the utility of the general impedance-matching method for the case of a microwave waveguide. Actually, far beyond that, we can enable maximum transmission of power in many other domains, via exploiting the doped ENZ material as the building block of the matching network. Here, we extrapolate the application of general impedance matching to the design of a near-zero-index antenna. As conceptually depicted in Fig. 4(a), we introduce open apertures at the boundary of the ENZ cavity to enable radiation into free space. However, the input reactance incurred by the evanescent fields at the edge of apertures may lead to a poor matching performance. To address this problem, dielectric dopants can be designed to compensate for the imaginary part of the input impedance of the aperture, and thus, allow better radiation efficiency. The constructed prototype of the near-zero-index antenna is shown in Fig. 4(b), where the air-filled rectangular waveguide at the cutoff frequency, f_p, is exploited to emulate the ENZ host, and the end of the ENZ cavity is open for radiation. A detailed description of the assembly procedure is presented in Appendix A. The input impedance of the rectangular aperture is extracted and shown in Fig. S5(a) within the Supplemental Material [38], indicating a feeding capacitive reactance of $2.2\eta_0$. To cancel the feeding reactance at frequency f_p, the effective relative permeability of the ENZ cavity (with a cross-section area of $h \times L_0$) in Fig. 4(b) has to be 0.35, according to Eq. (4). The size of the dopant is therefore determined by reference to Eq. (S5) within the Supplemental Material [38]. The 2D configuration of the proposed near-zero-index antenna and simulated magnetic field distribution are illustrated in Figs. S5(b) and

S5(c) within the Supplemental Material [38]. As shown in Fig. 4(c), the simulation and measurement results for the reflection amplitude in the presence of dopant are significantly reduced to below 0.1 at the design frequency. Despite a slight frequency detuning in the measurement, due to fabrication imperfection (minor unevenness of the width of the waveguide), the insensitivity of matching performance to the dopant's position is also evident from the experimental results, as demonstrated in Fig. 4(c). In addition, the radiation pattern is measured in a standard microwave anechoic chamber, and the results are gathered in Fig. S6 within the Supplemental Material [38], showing a quasi-omnidirectional pattern at the *x*-*z* cut plane and a "figure-of-eight"-shaped pattern, i.e., "∞", at the *y*-*z* cut plane with a peak realized gain of 2.3 dBi at the boresight ($+z$ direction).

Next, we introduce another interesting application of general impedance matching of delivering power to an arbitrarily shaped lossy dielectric particle. As illustrated in Fig. 4(d), absorbing particles with arbitrary shape are positioned in the ENZ host, while a dopant is designed to tune the impedance of the whole doped ENZ cavity, so as to match the feeding transmission line. In this manner, the input power can be fully sent into the doped cavity and delivered to absorbing particles. A detailed design is presented in Fig. 4(e), where an ENZ cavity with a cross-section area of $0.96\lambda_p^2$ includes an absorbing (i.e., lossy) particle with a relative permittivity of $10+0.1i$. The boundary of the absorbing particle is designed with a random-number generator; for detailed geometry information, please refer to Table S1 within the Supplemental Material [38]. The extracted input impedance at the interface of the ENZ host and feeding waveguide reads $(0.10-30.85i)\eta_0$, where the real part of input impedance is due to the loss of the absorbing particle. The imaginary part can be cancelled out, as before, by simply introducing an arbitrarily located dielectric dopant (the detailed matching procedure is presented in Section S6 within the Supplemental Material [38]). Once the input impedance is purely resistive, it can easily be transformed to η_0 by a simple quarter-wavelength impedance transformer [33], which is placed between the doped ENZ cavity and the air-filled feeding waveguide. The equivalent circuit is shown in the inset of Fig. 4(f). As seen from the simulation result, a perfect transmission of power to the absorbing particle is achieved, and changing the position of the dopant, as expected, does not influence the dip of the reflection coefficient. This method of illuminating or heating an absorbing particle, which can be considered as an efficient microwave or optical "oven", can be employed in a number of applications, including exciting the transition of a quantum material [41] and speeding up a biochemical reaction of, for example, a macromolecular cluster [42], and it may be of special interest to life sciences and material engineering.

V. EFFECTS OF MATERIAL LOSS

After providing proof-of-concept demonstrations of the general impedance-matching method, next we carry out a systematic study on the role of material loss in general impedance matching, which will determine the extrapolation of the proposed method to other physical systems. Without loss of generality, the configuration of the two-ENZ channel-matching network [shown in Fig. 5(a)] is used here as a case study to investigate the impact of loss from the photonic dopants, ENZ media, and surrounding metallic walls. The dielectric loss of the dopant directly contributes to the imaginary part of the effective permeability, which can essentially be treated as a resistance in series with the reactive matching component, according to Eq. (4). As illustrated in Fig. 5(b), we use the simulation results to evaluate the transmission amplitudes for cases of dielectric loss tangent of the dopant set as zero (thus, the imaginary parts of μ_{eff} of doped ENZ Ch. 1 and Ch. 2 are 0), 1% [thus, the imaginary parts of μ_{eff} of doped ENZ Ch. 1 and Ch. 2 calculated from Eq. (5) are $0.0009\mu_0$ and $0.0025\mu_0$, respectively], and 2% (thus, the imaginary parts of μ_{eff} of doped Ch. 1 and Ch. 2 are $0.0017\mu_0$ and $0.0050\mu_0$, respectively). The reduced transmission amplitude is caused by a slight mismatch and dissipation within the dopant. Next, we investigate the impact of loss of the ENZ media. To this end, we use a lossy Drude model, $\varepsilon_h(f) = 1 - {f_p}^2/(f^2 + if\gamma)$ (where γ denotes the collision frequency), to describe a realistic ENZ host around its plasmonic resonance. As seen in Fig. 5(c), the transmission peak at f_p is reduced to 0.75, when subjected to a collision frequency of around $0.06f_p$. Finally, the influence of loss in the surrounding metallic walls has to be discussed. To this end, instead of applying a perfect electric conductor boundary, we use a material with finite conductivity to surround the whole structure in Fig. 5(a), and the simulated transmission-amplitude responses for several different conductivities of metallic walls are gathered in Fig. 5(d). As seen, although the conductivity of the surrounding metallic material is decreased by five orders of magnitude, the operating band of transmission amplitude higher than 0.6 still remains over a range from $0.99f_p$ to $1.01f_p$. The simulated reflection coefficients considering different losses are reported in Fig. S8 within the Supplemental Material [38]. These parametric studies demonstrate the robustness of the general impedance-matching method to inevitable losses in real applications.

VI. CONCLUSION

We demonstrate the concept of general impedance matching via doped ENZ media. Theoretical analysis indicates that a doped ENZ region, despite having a finite size, acts as a pointlike lumped reactance with a highly controllable value. This property allows us to construct the

high-frequency distributed structures via elegant circuit-based design paradigms. As a unique merit of our design, via simply tuning the photonic dopants, we can tailor the dispersion of the effective permeability of doped ENZ medium; thus, a flexibly tailorable bandwidth of the matching networks built on doped ENZ regions is enabled. We present proof-of-concept experimental demonstrations at microwave frequencies, based on substrate-integrated waveguides, to validate the theory and design guidelines. Furthermore, the proposed impedance-matching scheme based on doped ENZ medium enables the opportunity to optimally guide power without limiting implementation to a specific type of load. This capability is demonstrated to feed a microwave component (the stepped waveguide), to enable efficient coupling of guided wave to free-space radiation, and to fully direct the power into an absorbing particle. With these advantages, our proposed scheme of general impedance matching might find applications in the fields of microwave engineering, optics, biomedicine, and materials science.

ACKNOWLEDGMENTS

Y.L. acknowledges partial support from the National Natural Science Foundation of China (NSFC) under Grant No. 61771280, as well as support from the Beijing National Research Center for Information Science and Technology, Tsinghua University, Beijing 10084, China. E.N. and N.E. acknowledge partial support from the US Air Force Office of Scientific Research (AFOSR) Multidisciplinary University Research Initiative (MURI) Grant No. FA9550-14-1-0389, and partial support from the Vannevar Bush Faculty Fellowship program sponsored by the Basic Research Office of the Assistant Secretary of Defense for Research and Engineering and funded by the Office of Naval Research through Grant No. N00014-16-1-2029.

APPENDIX A: EXPERIMENTAL SETUP AND MEASUREMENTS

The feeding waveguide in Fig. 3(c) is constructed on a 10-mm substrate with a dielectric constant of 2.5 and loss tangent of 0.025, while the stepped waveguide is fabricated using 10 and 1 mm substrates with a dielectric constant of 2.1 and loss tangent of 0.02. The metallized vias are drilled using standard planar circuit-board techniques, and then we glue the 10 and 1 mm substrates together. For exciting the feeding waveguide, a 50-Ω SMA connecter with a 9.5-mm long inner probe is armed at a distance of $\lambda_g/4$ (λ_g is the wavelength in the substrate) from the shorting vias that end the waveguide. The substrate-integrated waveguide on the 1 mm substrate is tapered into a 50 Ω microstrip line with a width of 2.4 mm, and terminated with the receiving SMA connector. The near-zero-index antenna shown in Fig. 4(b) is fabricated on a 5 mm substrate, with a dielectric constant of 2.2 and loss tangent of 0.003, via standard planar circuit-board techniques, and the 50-Ω SMA connecter, with a 4.8-mm long inner probe, is armed at a distance of $\lambda_g/4$ from the ending metallic vias.

[1] R. A. Shelby, D. R. Smith, and S. Schultz, Experimental verification of a negative index of refraction, Science **292**, 77 (2001).
[2] N. Engheta, An idea for thin subwavelength cavity resonators using metamaterials with negative permittivity and permeability, IEEE Antennas Wirel. Propagation Lett. **1**, 10 (2002).
[3] R. W. Ziolkowski and E. Heyman, Wave propagation in media having negative permittivity and permeability, Phys. Rev. E **64**, 056625 (2001).
[4] N. Engheta and R. W. Ziolkowski, *Metamaterials: Physics and Engineering Explorations* (IEEE-Wiley, New York, 2006).
[5] W. S. Cai, U. K. Chettiar, A. V. Kildishev, and V. M. Shalaev, Optical cloaking with metamaterials, Nat. Photonics **1**, 224 (2007).
[6] A. Alù and N. Engheta, Achieving transparency with plasmonic and metamaterial coatings, Phys. Rev. E **72**, 016623 (2005).
[7] Z. Jacob, L. V. Alekseyev, and E. Narimanov, Optical hyperlens: Far-field imaging beyond the diffraction limit, Opt. Express **14**, 8247 (2006).
[8] C. M. Soukoulis, S. Linden, and M. Wegener, Negative refractive index at optical wavelengths, Science **315**, 47 (2007).
[9] N. Yu, P. Genevet, M. A. Kats, F. Aieta, J. P. Tetienne, F. Capasso, and Z. Gaburro, Light propagation with phase discontinuities: Generalized laws of reflection and refraction, Science **334**, 333 (2011).
[10] A. Silva, F. Monticone, G. Castaldi, V. Galdi, A. Alù, and N. Engheta, Performing mathematical operations with metamaterials, Science **343**, 160 (2014).
[11] T. J. Cui, M. Q. Qi, X. Wan, J. Zhao, and Q. Cheng, Coding metamaterials, digital metamaterials and programming metamaterials, Light Sci. Appl. **3**, e218 (2014).
[12] N. Engheta, Pursuing near-zero response, Science **340**, 286 (2013).
[13] I. Liberal and N. Engheta, Near-zero refractive index photonics, Nat. Photonics. **11**, 149 (2017).
[14] I. Liberal and N. Engheta, The rise of near-zero-index technologies, Science **358**, 1540 (2017).
[15] M. Silveirinha and N. Engheta, Tunneling of Electromagnetic Energy Through Subwavelength Channels and Bends Using Epsilon-Near-Zero Materials, Phys. Rev. Lett. **97**, 157403 (2006).
[16] M. G. Silveirinha and N. Engheta, Theory of supercoupling, squeezing wave energy, and field confinement in narrow channels and tight bends using ϵ-near-zero metamaterials, Phys. Rev. B **76**, 245109 (2007).
[17] B. Edwards, A. Alù, M. E. Young, M. G. Silveirinha, and N. Engheta, Experimental Verification of Epsilon-Near-Zero Metamaterial Coupling and Energy Squeezing Using a Microwave Waveguide, Phys. Rev. Lett. **100**, 033903 (2008).

[18] M. G. Silveirinha and N. Engheta, Design of matched zero-index metamaterials using nonmagnetic inclusions in epsilon-near-zero media, Phys. Rev. B **75**, 075119 (2007).
[19] R. Liu, Q. Cheng, T. Hand, J. J. Mock, T. J. Cui, S. A. Cummer, and D. R. Smith, Experimental Demonstration of Electromagnetic Tunneling Through an Epsilon-Near-Zero Metamaterial at Microwave Frequencies, Phys. Rev. Lett. **100**, 023903 (2008).
[20] R. Maas, J. Parsons, N. Engheta, and A. Polman, Experimental realization of an epsilon-near-zero metamaterial at visible wavelengths, Nat. Photonics **7**, 907 (2013).
[21] A. M. Mahmoud and N. Engheta, Wave–matter interactions in epsilon-and-mu-near-zero structures, Nat. Commun. **5**, 5638 (2014).
[22] R. W. Ziolkowski, Propagation in and scattering from a matched metamaterial having a zero index of refraction, Phys. Rev. E **70**, 046608 (2004).
[23] Y. Li, S. Kita, P. Muñoz, O. Reshef, D. I. Vulis, M. Yin, M. Lončar, and E. Mazur, On-chip zero-index metamaterials, Nat. Photonics. **9**, 738 (2015).
[24] I. Liberal, A. M. Mahmoud, and N. Engheta, Geometry-invariant resonant cavities, Nat. Commun. **7**, 10989 (2016).
[25] R. Sokhoyan and H. A. Atwater, Quantum optical properties of a dipole emitter coupled to an ϵ-near-zero nanoscale waveguide, Opt. Express **21**, 32279 (2013).
[26] R. Fleury and A. Alù, Enhanced superradiance in epsilon-near-zero plasmonic channels, Phys. Rev. B. **87**, 2329 (2013).
[27] I. Liberal and N. Engheta, Nonradiating and radiating modes excited by quantum emitters in open epsilon-near-zero cavities, Sci. Adv. **2**, e1600987 (2016).
[28] A. Ciattoni, C. Rizza, and E. Palange, Extreme nonlinear electrodynamics in metamaterials with very small linear dielectric permittivity, Phys. Rev. A **81**, 043839 (2010).
[29] C. Argyropoulos, P. Y. Chen, G. D'Aguanno, N. Engheta, and A. Alù, Boosting optical nonlinearities in ϵ-near-zero plasmonic channels, Phys. Rev. B **85**, 045129 (2012).
[30] F. Monticone and A. Alù, Embedded Photonic Eigenvalues in 3D Nanostructures, Phys. Rev. Lett. **112**, 213903 (2014).
[31] M. G. Silveirinha, Trapping light in open plasmonic nanostructures, Phys. Rev. A **89**, 023813 (2014).
[32] I. Liberal, A. M. Mahmoud, Y. Li, B. Edwards, and N. Engheta, Photonic doping of epsilon-near-zero media, Science **355**, 1058 (2017).
[33] D. M. Pozar, *Microwave Engineering*, 2nd edn (John Wiley & Sons, New York, 1998).
[34] F. A. Jenkins and H. E. White, *Fundamentals of Optics*, 4th edn (McGraw-Hill, New York, 2001).
[35] P. R. West, S. Ishii, G. V. Naik, N. K. Emani, V. M. Shalaev, and A. Boltasseva, Searching for better plasmonic materials, Laser Photonics Rev. **4**, 795 (2010).
[36] Z. Zhou, Y. Li, H. Li, W. Sun, I. Liberal, and N. Engheta, Substrate-integrated photonic doping for near-zero-index devices, Nat. Commun. **10**, 4132 (2019).
[37] Y. Li, I. Liberal, C. D. Giovampaola, and N. Engheta, Waveguide metatronics: Lumped circuitry based on structural dispersion, Sci. Adv. **2**, e1501790 (2016).
[38] See the Supplemental Material http://link.aps.org/supplemental/10.1103/PhysRevApplied.13.034005 for guidelines to match the aperture antenna and the absorbing particle. Also, the impedance information of the stepped waveguide and a detailed discussion on the loss are given.
[39] COMSOL MULTIPHYSICS 5.0, COMSOL Inc. www.comsol.com.
[40] W. Rotman, Plasma simulation by artificial dielectrics and parallel-plate media, IRE Trans. Antennas Propag. **10**, 19 (1962).
[41] V. I. Klimov, A. A. Mikhailovsky, Su Xu, A. Malko, J. A. Hollingsworth, C. A. Leatherdale, H.-J. Eisler, and M. G. Bawendi, Optical gain and stimulated emission in nanocrystal quantum dots, Science **290**, 314 (2000).
[42] M. Larhed, C. Moberg, and A. Hallberg, Microwave-accelerated homogeneous catalysis in organic chemistry, Acc. Chem. Res. **35**, 717 (2002).